# Power Electronics Enabled Energy Management Systems

Giovanna Oriti, Alexander L. Julian, Nathan J. Peck
Electrical and Computer Engineering Dept.
Naval Postgraduate School
Monterey, CA, USA

***Abstract*—This paper demonstrates the functionality of a power electronics based energy management system (EMS). An EMS can optimize the use of energy sources and energy storage systems in microgrids. It can provide an intelligent interface with the main grid when the microgrid is connected, and it makes the microgrid fault tolerant by providing power to critical loads when the main power source fails. The EMS presented in this paper is developed on a digitally controlled power electronics system which can act as a current source or a voltage source depending on the situation. The EMS functionality is demonstrated by modeling, simulations and experimental measurements.**

## I. INTRODUCTION

Power electronics is a key enabling technology [1-3] to interface renewable energy sources to the grid and to provide the control features necessary to build a more controllable power system, often referred to as a "smart grid" [4,5]. Power converters enable electrical energy consumers to create microgrids that can operate autonomously or in parallel with the main grid. Digitally controlled power electronic converters can provide power flow metering and control, fault detection and correction [6-10], reliability improvements, enhanced electrical system security and other capabilities.

This paper presents the capabilities of a power electronics based Energy Management System (EMS) [11,12] including modeling and experimental prototyping. Aspects of electrical energy management include:

- Peak power control
- Active and reactive power metering and flow control
- Load, source and energy storage management
- Power quality control, reliability improvement and fault management.

A microgrid includes energy storage, energy sources, critical loads and non-critical loads. Energy storage is primarily in the form of batteries. Independent energy sources consist of a combination of photovoltaic panels (PV), gas or diesel generators, fuel cells, etc. The critical loads must be serviced at all times while the non-critical loads can be shed if power is insufficient. A block diagram showing how an EMS may interface with the main AC source and a microgrid is shown in Figure 1.

This paper is organized into seven sections. Following the Introduction, section II presents the functionality of the EMS as a main interface between a microgrid and the main power source. Different scenarios are presented to highlight the EMS control features and its ability to operate in grid connected and islanding modes. In section III the details of the EMS hardware and software design are illustrated and discussed. Section IV presents the physics based model developed to explore the EMS functionality. Laboratory hardware set up and experimental validation of the EMS functionality and model are presented in section V. Section VI investigates a scenario with additional loads using the validated model. Conclusions are presented in section VII.

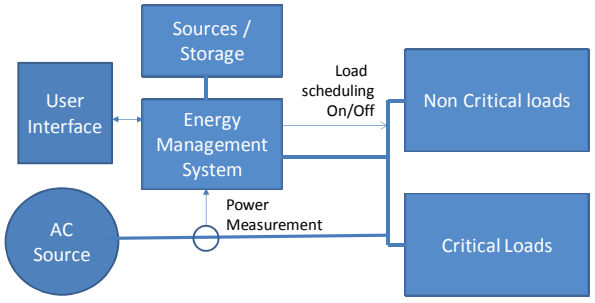


Figure 1. EMS interfacing to main grid and microgrid.

## II. EMS FUNCTIONALITY

The EMS creates the opportunity to manipulate power intelligently in a microgrid. Its functionality is demonstrated in this paper by modeling, simulation and experimental validation of the following scenarios:

1) Peak power control by tapping an energy storage system during high demand.

2) Islanding mode by necessity (loss of power) or by choice.

This project was sponsored by the Office of Naval Research and the Naval Postgraduate School.

3) Peak power control by non-critical load shedding during transients.

By accomplishing these goals the EMS can be very useful in grid connected systems where there is a limit on the user's power consumption. This limit maybe enforced by circuit breakers activated by thermal sensors. If the EMS keeps the source current below a set threshold at all times by load management and shedding, then the user can operate loads beyond the steady state power limits without worrying about the circuit breaker interrupting service. The EMS can also be useful when the user pays different rates for power delivered at different times of the day. In this case the EMS can manage the energy stored and energy drawn from the grid to reduce consumption when the power rates are higher.

On an autonomous microgrid, where one or more generators are used to power different loads, the EMS allows derating of the generator by controlling the peak rms current drawn. It can also ensure power to critical loads is maintained during a fault by managing energy storage.

Three scenarios are illustrated in Figure 2 where a microgrid with a single phase power source and a battery pack is used to demonstrate the functionality of the EMS. The battery pack can be recharged either from the grid or from other power sources such as PV cells, etc. Two sets of loads, one critical and the other non-critical are used to illustrate the EMS functionality. The first scenario shows how the peak rms current drawn from the source is limited by the EMS when the critical load increases. In this case the EMS behaves as a current source, providing the additional load current. The second scenario demonstrates islanding mode of operation when the load is so light that the battery can provide all its current. This scenario may also occur when there is a fault in the main power grid or if the power quality decreases below a level which is required by critical loads. In this case, the EMS inverter operates as a voltage source. The third scenario shows how the EMS can shed a non-critical load when the critical load increases, thus keeping the source rms current below a set limit. All three scenarios are demonstrated in this paper with experimental measurements and simulations.

The EMS control algorithm was developed with the following goals, listed here in order of priority:

1. Power must be available to the critical loads at all times. As an example, if the main power supply (grid) is down, then battery power will be used to support critical load operation.
2. Reduce the peak power absorbed by the microgrid by using battery power and by non-critical load shedding.
3. Maximize the state of charge of the battery.
4. Make power available to non-critical loads.

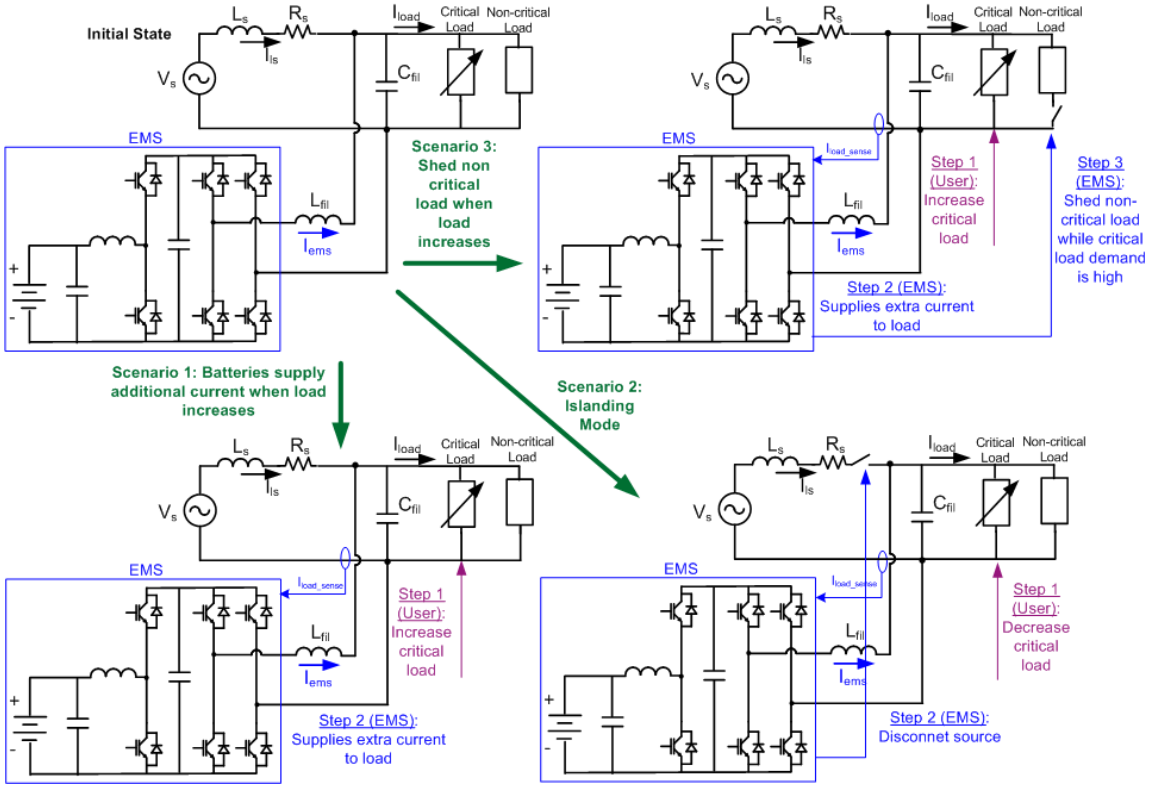


Figure 2. Scenarios used to demonstrate EMS functionality.

## III. EMS HARDWARE

The power electronics based power conversion system shown in Figure 3 and Figure 4was designed to support laboratory development and rapid experimental validation for research and thesis projects [13-16] at the Naval Postgraduate School. It includes a field programmable gate array FPGA development board [17] with input/output (I/O) ports, an insulated gate bipolar transistor (IGBT) power module, power supply, voltage/current sensors, analog/digital (A/D) converters, transistor transistor logic (TTL) interface and a USB interface to communicate with a PC as shown in the schematic of Figure 3. A Joint Test Action Group (JTAG or IEEE Standard 1149.1) programming cable interfaces the FPGA development board to a PC and is used to program the FPGA. The software development tool used for the FPGA is Simulink [18] with the addition of Xilinx System Generator software [19] which compiles the Simulink model to create VHDL code. The interface functionality of Figure 3 is realized by two printed circuit boards (PCBs) mounted above and below the FPGA development board as shown in Figure 4. The bottom PCB includes the power components such as the IGBT Integrated Power Module (IPM), current and voltage sensors, passive components and DC power supply. The IGBT IPM includes six diodes, six IGBTs and the gate drive circuits in the standard three phase three legs configuration. For the EMS presented in this paper two legs are used in a single phase H-bridge inverter configuration while the third leg is used to interface with the battery pack. The PCB mounted on top of the FPGA development board includes a USB interface chip, USB connector to interface with the PC, A/D converters, voltage level shifters and several other connectors to interface with the other boards.

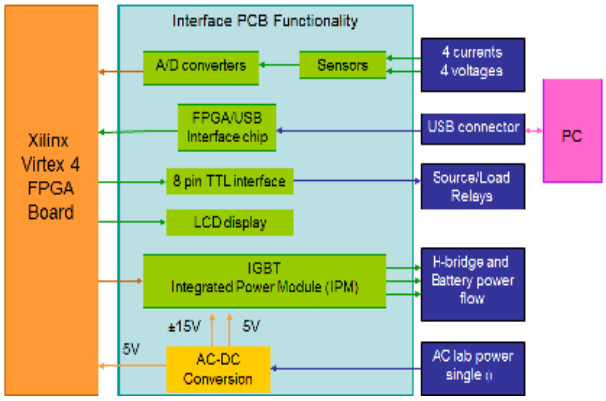


Figure 3. EMS electronics block diagram (UPDATED)

## IV. EMS MODELING

A physics based model of the EMS was developed and implemented using Simulink software [18]. Figure 5 shows the top level Simulink model block diagram including the EMS, critical and non-critical loads, and the main power source. The circuit schematic of the Simulink model is shown in Figure 6.

The EMS block includes the logic algorithm which controls the loads intelligently. The logic algorithm, seen in Figure 7, is implemented using a Matlab function block. The load current, the status of the non-critical load, the presence of the utility power source and a disable/clear pushbutton toggle are inputs to the Matlab function block. The Matlab function block outputs the signals that allow the EMS to provide stored energy as a current source or voltage source, and to shed or restore non-critical loads.

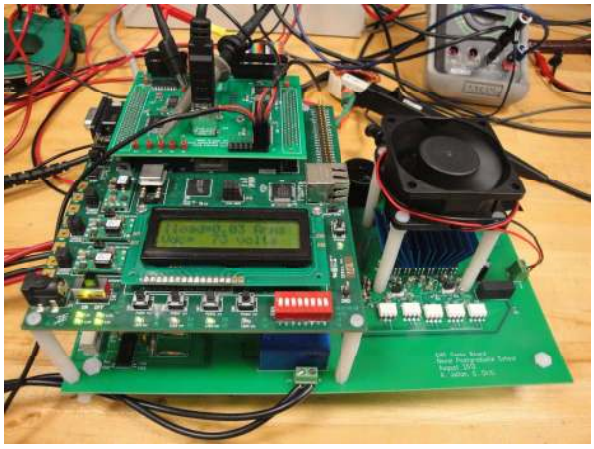

Figure 4. FPGA based EMS electronics.

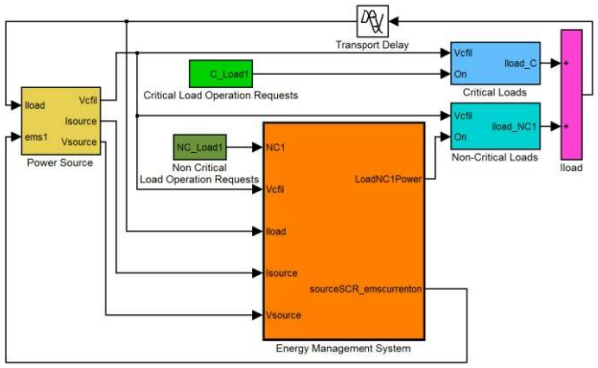


Figure 5. Simulink model block diagram.

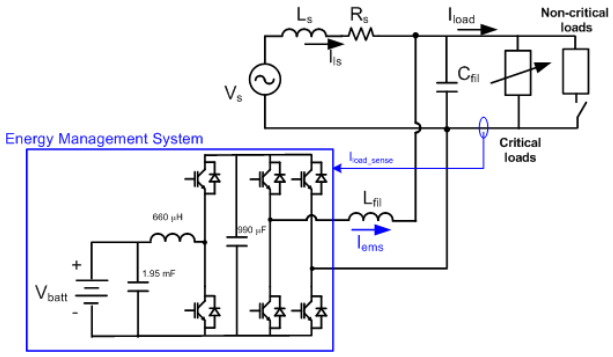


Figure 6. Circuit schematic implemented in the Simulink model

The Matlab function block uses the rms value of the load current and the source voltage, which are calculated in the EMS block using (1)

$$I_{rms} = I_{avg} \frac{\pi}{2\sqrt{2}} \quad (1)$$

This equation uses the relationship between (2) and (3)

$$I_{rms} = I_P / \sqrt{2} \tag{2}$$

$$I_{avg} = \frac{2I_p}{\pi} \tag{3}$$

Where $I_p$ is the peak current for a sinusoidal current. Equation (3) is applicable to a rectified sine wave whose average value is found using (4).

$$I_{avg} = \frac{2}{T}\int_0^{T/2} I_p \sin(\omega t)\,dt = \frac{2I_p}{\pi} \quad \text{where } \omega = \frac{2\pi}{T} \tag{4}$$

The Simulink model determines the average value by taking the absolute value of the input and sending it through two 5Hz low pass filters. The average value is then multiplied by the constant to obtain the rms value, as shown in (1).

The peak power control load shedding logic is shown in Figure 7 for a single non-critical load scenario. The logic is dependent on the status of the source, the load current, the status of the non-critical loads and a disable/clear push button toggle. The value of the load current threshold to shed non-critical loads is dependent on the status of the source. This value is referred to as $I_{max}$. If the source is not available, due to a fault in the main power grid or poor power quality, then $I_{max}$ is set to a lower value that supports sustained islanding operations. If the source is powering the microgrid, then $I_{max}$ is set to a higher value that supports peak power control. The same approach is used for the load current threshold to restore non-critical loads that have been shed, which is referred to as $I_{maxoff}$. If the source is not available then $I_{maxoff}$ is set to a lower value than if the source is powering the microgrid. When the source is available $I_{max}$ is set to provide additional current from the separate DC source prior to shedding any non-critical loads. If at any time the load current is between $I_{max}$ and $I_{maxoff}$ the EMS maintains the non-critical loads' previous state. A push button toggle input is also incorporated into the logic. This allows a user to disable the load shedding capability or to clear a load shedding transient that did not have a steady state load current below the $I_{maxoff}$ threshold.

The algorithms for the critical load and non-critical load blocks in Figure 5 are identical in implementation, but use different values. The first input is the voltage across the load, $V_{cfil}$. The second input is the on/off signal. The output is the current through the load. The output of the blocks is computed using Ohm's law:

$$I_{load} = V_{cfil} / R \tag{5}$$

where $R$ is the resistance of the load. The "Power Source" block in the Simulink model represents the utility power source. It implements the following differential equations with respect to Figure 6 ($s$ represents differentiation in (6-9)):

$$V_{source} - sL_s I_{source} - R_s I_{source} - V_{cfil} = 0 \tag{6}$$

$$I_{source} = \frac{1}{sL_s}\left(V_{source} - V_{cfil} - R_s I_{source}\right) \tag{7}$$

$$I_{cfil} = I_{source} - I_{load} + I_{ems} \tag{8}$$

$$V_{cfil} = \frac{1}{sC_{cfil}} I_{cfil} = \frac{1}{sC_{cfil}}\left(I_{source} - I_{load} + I_{ems}\right) \tag{9}$$

The EMS current, $I_{ems}$, is implemented in the EMS block.

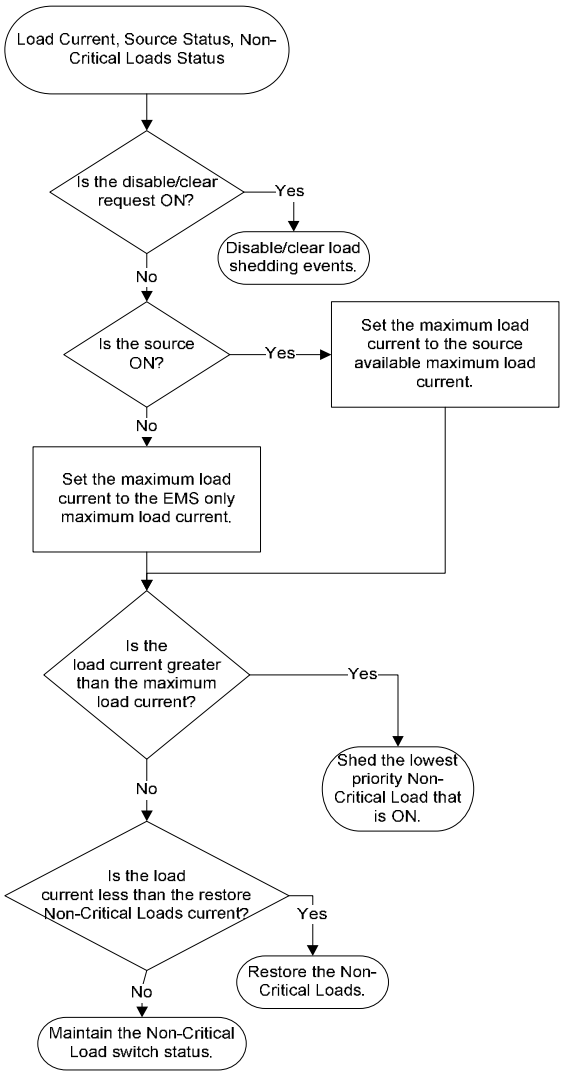


Figure 7: EMS load control logic

## V. EMS Experimental Demonstration

An EMS was set up in the lab using the hardware described in section III. The circuit shown in Figure 6 was simulated using the Simulink model and validated in the lab. The source voltage is $V_s$ =120Vrms, the battery pack voltage is $V_{batt}$=72Vdc and it is boosted to create a 200 Vdc bus for the H-bridge inverter. The EMS output filter includes the capacitor $C_{fil}$ = 13.2 μF, and the inductor $L_{fil}$ = 1.16 mH. The two loads are purely resistive. The critical load resistance is variable and consists of three parallel resistors measuring

1200Ω, 600Ω, and 300Ω, which can be switched in and out of the circuit. The non-critical load resistance is 400Ω.

### *A. Peak power control with main grid connected*

Peak power control is achieved in the lab by controlling the rms current in the load which affects the source current.

With the microgrid connected to the main power source the first scenario of Figure 2 was implemented in the laboratory. In this scenario the H-bridge inverter in the EMS is controlled as a current source and provides half of the load current, reducing the peak power drawn from the source without load shedding. This scenario is demonstrated by the experimental measurements shown in Figure 8. The waveforms show that when the critical load increases ($I_{load}$ increases in Figure 8), the total load current, $I_{load}$, is increased and the EMS turns on in current mode to provide half of the load current ($I_{ems}$= ½ $I_{load}$). There is a delay between the load increase and the EMS turning on due to the rms current computation algorithm.

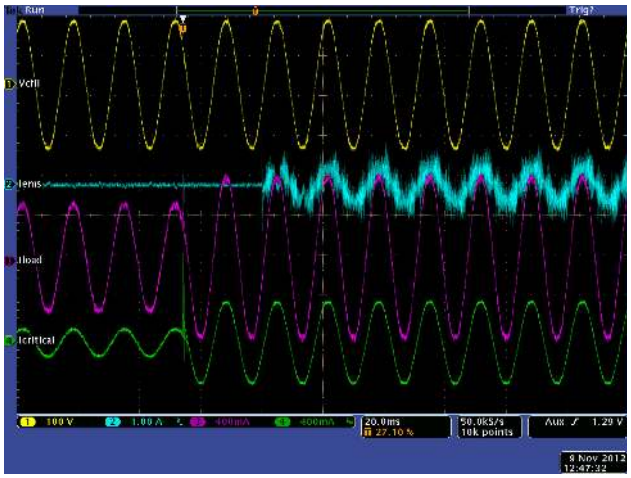


Figure 8. Experimental measurements demonstrating peak current control with EMS providing some of the load current.

The third scenario of Figure 2, demonstrating non-critical load shedding, was implemented in simulations and then validated in the lab. In this scenario the critical load resistance was decreased from 400 Ω to 171 Ω. The resulting load rms current was greater than the load current shedding threshold, $I_{max}$, and the non-critical load was shed. For this experiment, $I_{max}$ =0.78A and $I_{maxoff}$ =0.32A in the load management algorithm described in section IV. Figure 9 shows the load shedding transient as simulated using the Simulink model presented in section IV. The experimental waveforms for the same scenario as implemented in the laboratory set up are shown in Figure 10.The critical load current, $I_{critical}$, is never interrupted (bottom waveform). The load current, $I_{load}$, which includes the critical load current, is reduced when the measured load current exceeds the upper threshold programmed in the FPGA by shedding the non-critical load. The EMS is in current control mode, $I_{ems}$, and is programmed to provide half of the load current at all times in order to reduce the peak current from the source. The top waveform, $V_{cfil}$, is the AC bus voltage across the capacitor, $C_{fil}$, in Figure 6.

In both figures, approximately 70ms of delay between the critical load increase and the non-critical load shedding is seen. The delay between the two events is due to the time required for the load current rms value to update.

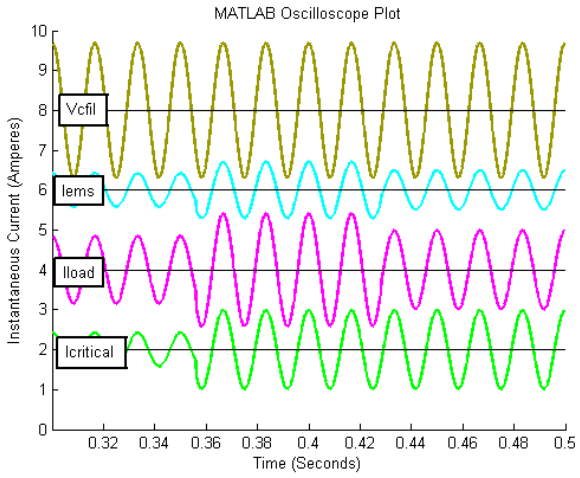


Figure 9. Simulated plots of load shedding scenario with grid connected. Vcfil is 1/100$^{th}$ of actual value and the units are volts. Each waveform is offset from zero by multiples of 2.

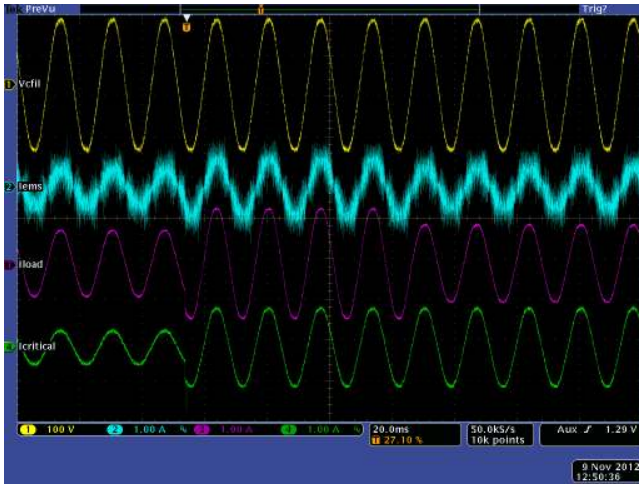


Figure 10. Experimental plots of load shedding scenario with grid connected.

Simulations and experimental measurements are in good agreement except for the high frequency ripple in the experimental EMS current waveform. Such ripple is absent in the simulated waveform because the model of the H-bridge inverter in the simulation does not include the power converter's switching behavior. Future work will include a more detailed physics based model of the system and power quality management will be addressed to reduce the ripple.

### *B. Peak power control in islanding mode of operation*

Load shedding and load restoration events while the microgrid is operating as an island are demonstrated in Figure 11 and Figure 12 respectively. The critical load resistance was decreased from 1200Ω to 400Ω in Figure 11, thus causing the total load current, $I_{load}$, to increase beyond the threshold, $I_{max}$.

The EMS is providing all of the load current, so it reacts by shedding the non-critical load. Note that the critical load is undisturbed while the critical load is shed.

The critical load resistance was increased from 400 Ω to 1200 Ω in Figure 12. This causes the EMS to turn on the non-critical load since the total load current falls below the $I_{maxoff}$ threshold. Note that the time delay during load restoration, as seen in Figure 12, is approximately 20ms faster than seen during load shedding.

For these experiments the variables for the load control algorithm described in section IV were $I_{max}$ =0.32A and $I_{maxoff}$ = 0.16A.

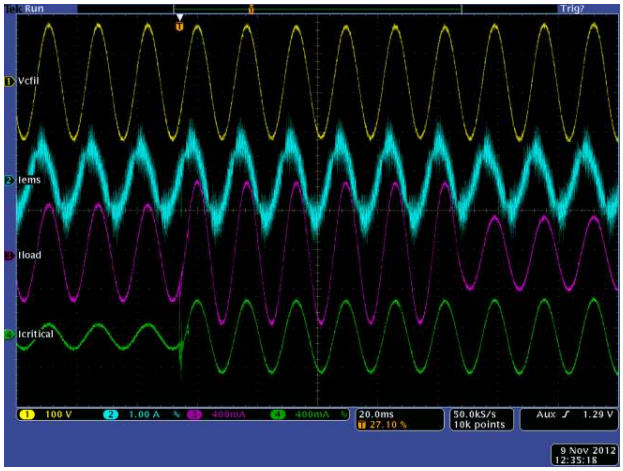


Figure 11. Experimental plots of load shedding in islanding mode (main grid disconnected).

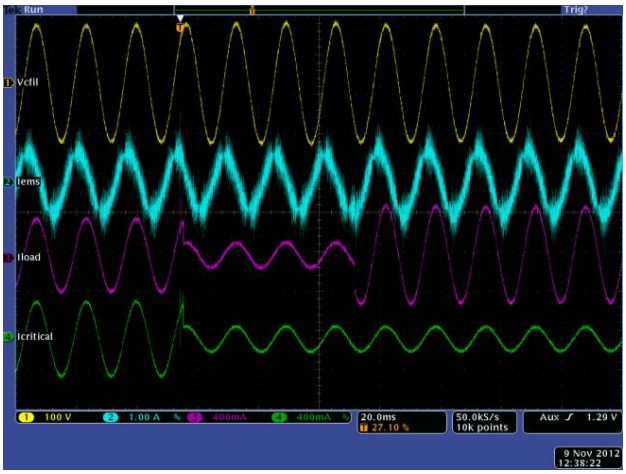


Figure 12. Experimental plots of non-critical load restoration in islanding modeof operation.

### C. *EMS providing power to critical loads when grid fails*

In order to provide power to critical loads when the main grid fails, the EMS detects grid failure and acts as a voltage source for the critical loads. This case is labeled "scenario 2" in Figure 2. The voltage and current waveforms measured when the main grid is disconnected and the EMS begins operating as a voltage source are shown in Figure 13. Before the power failure, the non-critical load was on and the critical load was on with a resistance of 400 Ω. After the grid is disconnected and the EMS provides the voltage to the microgrid, the non-critical load is shed and only the critical load is serviced. The response time of the EMS will be improved in future experiments.


Figure 13. Experimental plots of main power source failure and EMS picking up the critical load.

## VI. EMS Managing More Complex Loads

The Simulink model presented in section III was experimentally validated in section IV. It is now a tool that can be used to design more complex systems and to predict their behavior. In particular scenarios with more than two loads, which can be non-resistive, can be simulated to demonstrate more aspects of the EMS functionality.

The circuit in Figure 14 was modeled and simulated using Simulink. The circuit consists of four loads, two critical and two non-critical. The two critical loads are a rectifier and a resistor. The two non-critical loads are a motor and a resistor. The EMS prioritizes the non-critical motor load above the non-critical resistive load. The load shedding current threshold, $I_{max}$, is set to 43A. The current threshold to provide EMS current is half of the load shedding threshold or 21.5 A. The threshold to restore shed loads, $I_{maxoff}$, is the load shedding threshold minus the peak non-critical load current which is 16 A. Both resistive loads turn on at 0.11 seconds. The rectifier load turns on at 0.4 seconds and off at 3 seconds. The motor load turns on at 0.6 seconds and remains on for the rest of the simulation.

Three sets of simulations were performed to show the behavior of the system with and without the EMS. In the first simulation, the EMS is fully operational, providing current from the battery pack and performing load shedding. The second simulation shows the case where the EMS supplies current to the loads but does not perform load shedding. The third simulation shows what the microgrid waveforms look like when the EMS is completely disabled.

The rms currents are shown in Figure 15 when the EMS is fully operational. The rms values of the source current, $I_{source}$, load current, $I_{load}$, and EMS current, $I_{ems}$, are plotted together with the load current thresholds. When the rectifier load turns

on at 0.4 seconds, the supplementary EMS current turns on to reduce the current drawn from the source. The subsequent start of the motor at 0.6 seconds increases the load current above the load shedding threshold. The EMS sheds the non-critical resistive load as seen in Figure 16. This reduces the load current below the load shedding current threshold, $I_{max}$, during the motors start up cycle. The motor startup resistors secure at approximately two seconds.

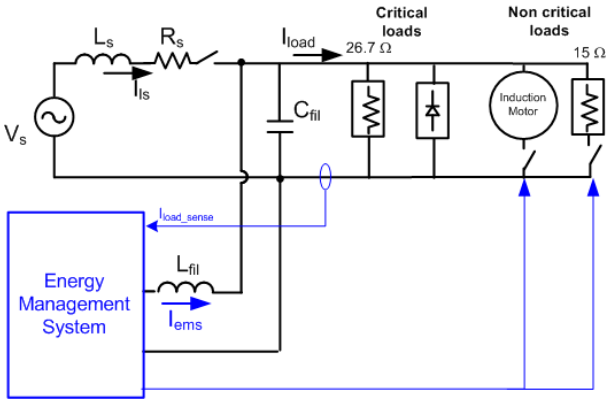


Figure 14. Circuit schematics of simulated scenario with four loads.

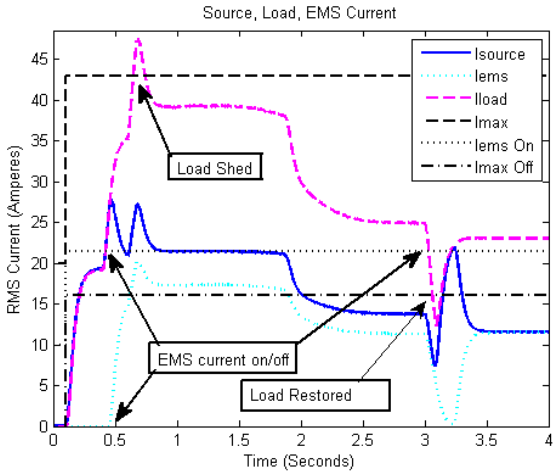


Figure 15. Simulation current plots when the EMS is fully operational.

The circuit reaches a steady state condition just before three seconds and then the rectifier load turns off. The load current drops below the EMS current threshold and the non-critical load restoration threshold, $I_{maxoff}$. This permits the non-critical resistive load to be restored. As a result of restoring the non-critical resistive load, the EMS current turns on again.

The non-critical load restoration threshold, $I_{maxoff}$, is the load shedding threshold minus the peak non-critical load current. This threshold was chosen to prevent non-critical load oscillations when shedding loads. A non-critical load restoration threshold above this value could result in non-critical load oscillations if both non-critical loads were shed. The drawback of such a low restoration threshold is a system that is not maximizing the power available to it. Specifically, non-critical loads whose operation would not result in the load current exceeding $I_{max}$ are still prevented from operating without operator action. Operator action to restore shed non-critical loads was implemented with a disable/clear toggle pushbutton for EMS load shedding.

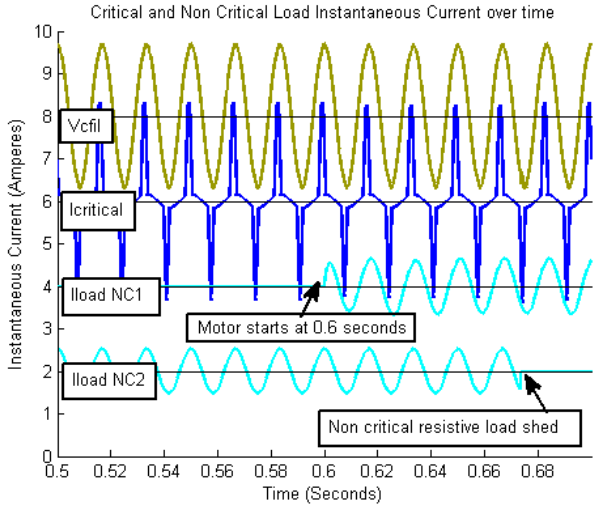


Figure 16. Simulated waveforms showing a lower priority non-critical load being shed. $V_{cfil}$ is 1/100th of actual value. Currents are 1/40th of actual values. Each waveform is offset from zero by multiples of 2.

When operating without EMS load shedding, the supplementary current from the EMS turns on as before, but the load current exceeds $I_{max}$. Figure 17 shows the plots for this simulation without load shedding. The disadvantage of operating without load shedding is that the system can potentially exceed a maximum source current resulting in loss of power to the entire system instead of just to the non-critical loads.

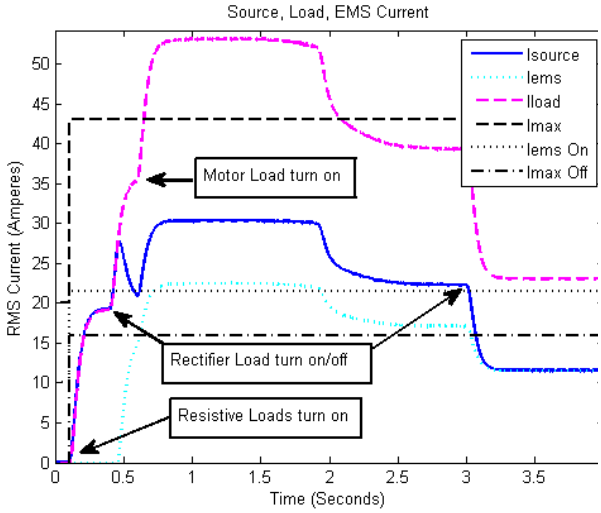


Figure 17. Simulation plots without load shedding.

The plots resulting from the simulations without the EMS are shown in Figure 18. In this case the source must support all the loads at any time. The plots clearly show that $I_{load} = I_{source}$. The disadvantage of such a system is the peak power demand it places on the power source. It requires a power

source that is sized to support the peak power demand, but typically operates at a lower demand that is less efficient.

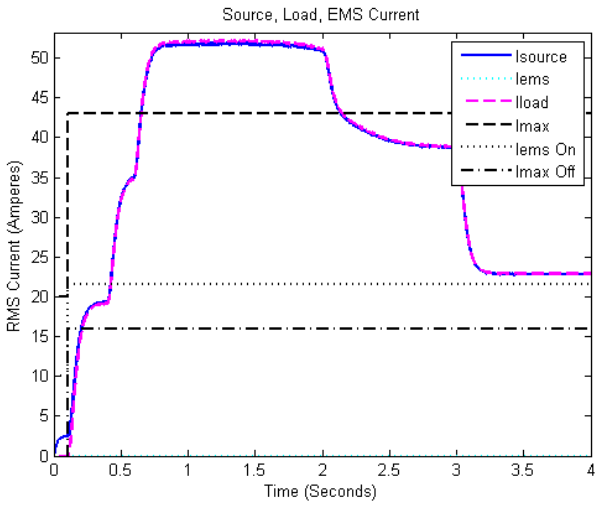


Figure 18. Simulation plots with the EMS disabled.

## VII. CONCLUSIONS

In this paper the functionality of a power electronics based EMS is presented together with its application. The technical challenges associated with the experimental implementation of typical scenarios are addressed and presented. Additionally physics based models are developed, experimentally validated and then used to study the functionality of the EMS when operating in more complex systems. Several functional details have been identified that can affect the EMS performance:

- Response time of the RMS calculation
- Setting thresholds to avoid loads turning on and off repetitively
- The power quality when transitioning to islanding mode
- The power quality with non-linear loads when in islanding mode

An EMS can significantly improve power reliability, availability, efficiency and quality and these advantages will be explored more in future work.

## REFERENCES


[1] M. Godoy Simões, R. Roche, E. Kyriakides, A. Miraoui, B. Blunier, K. McBee1, S. Suryanarayanan, P. Nguyen and P. Ribeiro, "Smart-Grid Technologies and Progress in Europe and the USA", in *Proc. of IEEE Energy Conversion Conference and Expo*, ECCE 2011, Phoenix, AZ, Sep, 2011.

[2] R. Carnieletto, D.I. Brandão, S. Suryanarayanan, F.A. Farret, M.G. Simões, "Smart Grid Initiative", *IEEE Industry Applications Magazine*, vol17, no.5, Sep/Oct 2011.

[3] D. Boroyevich, I. Cvetković, D. Dong, R. Burgos, F. Wang, F. Lee, "Future Electronic Power Distribution Systems – A contemplative view ", in *Proc. of IEEE 12th International Conference on Optimization of Electrical and Electronic Equipment*, OPTIM 2010.

[4] DOE Smart Grid Initiative. http://energy.gov/oe/technology-development/smart-grid

[5] Massoud Amin, S. and Wollenberg, B.F., "Toward a smart grid: power delivery for the 21st century." *Power and Energy Magazine*, IEEE, Sept.-Oct. 2005, Issue 5, Vol. 3.

[6] P.K. Lee and L.L. Lai, "Smart Metering in Micro-Grid Applications", in *Proc. of IEEE Power and Energy Society General Meeting*, 2009.

[7] R. Majumder, A. Ghosh, G. Ledwich, and F. Zare, "Power Management and Power Flow Control With Back-to-Back Converters in a Utility Connected Microgrid", *IEEE Transactions in Power Systems*, Vol. 25, No. 2, MAY 2010.

[8] F.Z. Peng, Y.W. Li, L.M. Tolbert, "Control and Protection of Power Electronics Interfaced Distributed Generation Systems in a Customer-Driven Microgrid", in Proc. of *IEEE PES General Meeting*, 2009.

[9] F. Blaabjerg, Z. Chen, and S. B. Kjaer, "Power Electronics as Efficient Interface in Dispersed Power Generation Systems", *IEEE Trans. on Power Electronics*, vol. 19, pp. 1184-1194, Sept. 2004.

[10] P. Sun, C. Liu, J. Lai, C. Chen, "Grid-Tie Control of Cascade Dual-Buck Inverter with Wide-Range Power Flow Capability for Renewable Energy Applications", *IEEE Trans. on Power Electronics*,vol.27 no.4, April 2012.

[11] S. Chakraborty, M. D. Weiss, M. G. Simões, "Distributed Intelligent Energy Management System for a Single-Phase High-Frequency AC Microgrid", *IEEE Trans. on Industrial Electronics*, vol. 54, no.1, Feb 2007.

[12] E. Barklund, N. Pogaku, M. Prodanovic´, C. Hernandez-Aramburo, T. C. Green, "Energy Management in Autonomous Microgrid Using Stability-Constrained Droop Control of Inverters", *IEEE Trans. on Power Electronics*, vol. 23, no. 5, Sep 2008.

[13] J. E. O'Connor, Field Programmable Gate Array Control of Power Systems in Graduate Student Laboratories, Master Thesis, Naval Postgraduate School, Monterey, CA, March 2008.

[14] G. Oriti, D. Zulaica, A.L. Julian, R. Cristi, "Hardware Laboratories for Power Electronics and Motor Drives Distance Learning Courses" in *Proc. of IEEE 2nd Energy Conversion Conference and Expo* (ECCE) 2010, Atlanta, GA, Sept 2010.

[15] G. Oriti, A.L. Julian, "Three Phase VSI with FPGA Based Multisampled Space Vector Modulation", *IEEE Trans. on Industry Applications*, Vol. 47, No.4, Jul/Aug 2011.

[16] G. Oriti, A.L. Julian, D. Zulaica, "Doubly Fed Induction Machine Drive Distance Learning Laboratory for Wind Power and Electric Ship Propulsion Applications", in *Proc. of IEEE 3rd Energy Conversion Conference and Expo* (ECCE) 2011, Phoenix, AZ, Sep 2011.

[17] Xilinx® "Avnet Virtex-4 LC Development Board", online at: http://www.xilinx.com/products/devkits/DS-KIT-4VLX25LC.htm.

[18] Simulink® by MathWorks [Online] http://www.mathworks.com/products/simulink/

[19] Xilinx "System Generator for DSP -Getting Started Guide" Release 10.1 March, 2008, [Online]. Available: http://www.xilinx.com/support/sw_manuals/sysgen_gs.pdf